[10] Tseng, R. C., "Flat Plate Boundary Layer Studies in a Partially Ionized Gas," AS-69-14, 1969, Univ. of California, Berkeley, Calif.

[11] Sonin, A. A., "Free Molecule Langmuir Probe and its Use in Flowfield Studies," *AIAA Journal*, Vol. 4, No. 9, Sept. 1966, pp. 1588–1596.

[12] Kirchhoff, R. H., Peterson, E. W., and Talbot, L., "An Experimental Study of the Cylindrical Langmuir Probe Response in the Transition Regime," AS-69-13, 1969, Univ. of California, Berkeley, Calif.

[13] deLeeuw, J. H., "Electrostatic Plasma Probes," *Physico-Chemical Diagnostics of Plasmas*, T. P. Anderson et al., eds., Northwestern University Press, Evanston, Ill., 1963, pp. 65–95.

[14] Chen, F. F., "Electrostatic Probes," *Plasma Diagnostic Techniques*, R. H. Huddlestone and S. L. Leonard, eds., Academic Press, New York, 1965, pp. 113–119.

[15] Laframboise, J. G., "Theory of Spherical and Cylindrical Langmuir Probes in a Collisionless, Maxwellian Plasma at Rest," 100, 1966, Institute for Aerospace Studies, Toronto.

[16] Graf, K. A., "The Determination of Spatially Non-uniform Electron Density Distribution," 108, 1965, Institute for Aerospace Studies, Toronto.

[17] Johnson, E. O. and Malter, L., "A Floating Double Probe Method for Measurement in Gas Discharges," *Physical Review*, Vol. 80, No. 1, Oct. 1, 1950, pp. 58–68.

[18] Kiel, R. E., "Electrostatic Probe Theory for Free Molecular Cylinders," *AIAA Journal*, Vol. 6, No. 4, April 1968, pp. 708–712.

[19] Kirchhoff, R. H., "An Experimental Investigation of the Shock Structure in a Partially Ionized Gas," AS-69-S, 1969, Univ. of California, Berkeley, Calif.

[20] Bienkowski, G. K., "Electrostatic Sheath in a Weakly Ionized Gas," *The Physics of Fluids*, Vol. 10, No. 2, Feb. 1967, pp. 381–390.

[21] Brown, S. C., *Introduction to Electrical Discharges in Gases*, 1st ed., Wiley, New York, 1966.

[22] Chapman, D. R. and Rubesin, M. W., "Temperature and Velocity Profiles in the Compressible Boundary Layer with Arbitrary Distribution of Surface Temperature," *Journal of the Aeronautical Sciences*, Vol. 16, No. 9, Sept. 1949, pp. 547–565.

[23] Hinnov, E. and Hirschberg, J. G., "Electron-Ion Recombination in Dense Plasmas," *Physical Review*, Vol. 125, No. 3, Feb. 1, 1962, pp. 795–801.

[24] Brundin, C. L., "The Application of Langmuir Probe Technique to Flowing Ionized Gases," AS-64-9, 1964, Univ. of California, Berkeley, Calif.

[25] Dix, D. M., "Energy Transfer in a Partially Ionized, Two-Temperature Gas," ATN-64(9232)-1, 1964, Aerospace Corp., El Segundo, Calif.

[26] Spitzer, L., *Physics of Fully Ionized Gases*, 2nd ed., Interscience, New York, 1962, pp. 143–145.

[27] Holt, E. H. and Haskell, R. E., *Foundations of Plasma Dynamics*, 1st ed., Macmillan, New York, 1965, p. 270.

[28] Chen, C. J., "Partition of Recombination Energy in the Decaying Rare Gas Plasmas," *Physical Review*, Vol. 163, No. 1, Nov. 5, 1967, pp. 1–7.

Cathode Region of a Quasi-Steady MPD Arcjet

P. J. Turchi[*] and R. G. Jahn[†]

Princeton University, Princeton, N.J.

An MPD discharge is examined near the cathode of a 2.5 Mw, quasi-steady, self-field arcjet. High-speed photography shows a concentration of arc luminosity in the cathode region, while detailed measurements with electric and magnetic field probes indicate that 85% of the total arc power is deposited within one base diameter of the cathode surface. Ion energies are shown to be proportional to the voltage drop in the cathode region even though current conduction is accomplished primarily by electrons in a tensor manner. It is found that a high-speed plasma flow is delivered to the cathode, where it is converted into a useful exhaust jet in a thin, high-density layer at the cathode surface. Local measurements of electron temperature and estimates of electron density, made within the discharge and exhaust jet using a twin Langmuir probe technique, indicate a nearly uniform electron temperature of about 1.5 ev throughout the quasi-steady arcjet flow.

I. Introduction

OUR purpose here is to understand the physical processes involved near the cathode of an MPD arcjet. Interest in such processes derives from a desire to achieve logical guidelines for the design of an optimum electric thruster of this type for space applications. We shall be particularly concerned with the mechanics of current conduction and plasma acceleration in the vicinity of the cathode, and the transfer of electrical energy to the plasma in this region.

II. Experimental Program

Experiments inside steady MPD arcjets are ordinarily prohibited by the small volume of the arc chamber and the violence of arc operation. Understanding of MPD processes has thus been limited to inferences made from various terminal properties such as total voltage, current, thrust, etc., supplemented by optical measurements of arc-luminosity distribution, and species existence and temperature. We seek to improve this situation by a series of detailed measurements within a high power, large radius, quasi-steady arcjet.

Experimental Facility

By operating an arcjet with a short pulse of high current, we are able to avoid the experimental difficulties of poor interior access and instant probe destruction. Higher currents allow us to scale the arc-chamber dimensions to maintain the intensity of MPD operation in a larger volume. Thus, for a

cylindrical system, a factor of 10 increase in current from 2000 amp to 20,000 amp permits a similar change in chamber diameter from 1 cm to 10 cm.[1] At the same time, the short duration of the current pulse limits energy transfer to modest amounts even at the higher power levels involved, allowing small, uncooled probes to survive within the arc chamber.

The design philosophy of the quasi-steady arcjet and details of the construction of the facility used here are discussed by Clark.[1] Briefly, our apparatus consists of a 5-in.-diam, 2-in.-high chamber in which a diffuse arc forms between a conical tungsten cathode and a coaxial aluminum anode (Fig. 1). For the experiments discussed here, the arc operates at 17.5 ka, with a constant argon mass inflow of 5.9 g/sec, and exhausts into a Plexiglas vacuum vessel maintained at 2×10^{-5} torr. Current is supplied by a capacitor bank arranged as an LC-ladder network to provide a flattopped current pulse for 170 μsec. Argon flows into the arc chamber through six choked orifices from a high-pressure reservoir created at the driven-section end wall of a vacuum shock tube. The current pulse is initiated in the chamber when the mass flow has attained a steady level. Some 30 μsec after discharge initiation, total voltage, current, magnetic field distribution, and over-all arc appearance achieve a steady state which is maintained until the current decreases at the end of the pulse. Recent experiments[2] indicate that this situation is representative of millisecond quasi-steady operation.

Previously reported measurements[3] in the downstream exhaust jet at this current and mass flow condition indicate velocities of about 2×10^4 m/sec, electron temperatures of 1.4 ev and ion temperatures on the order of 10 ev.

Visual Observations

Qualitative information on the nature of the arc in the cathode region is provided by photography through a high-speed Kerr cell shutter. A portion of the arc-chamber side wall is removed allowing the entire discharge region to be viewed through the glass insulator. The shutter is triggered at a known time in the current pulse and remains open for 5 μsec. Both color slides and black and white prints have been obtained in this manner showing the initiation and development of the discharge as the current to the chamber increases, and the establishment of a quasi-steady luminosity distribution when the current level becomes constant. Figure 2 is a photograph of the discharge at a representative time during quasi-steady operation. The concentration of luminosity within one (base) diameter of the cathode surface and in a conical region extending from the cathode tip suggests the importance of cathode processes to arcjet operation.

In the color photographs, the region near the base of the cathode appears bright green, while the region downstream of
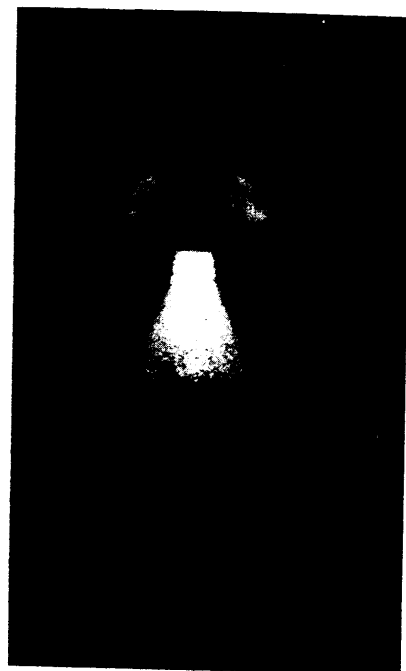

Fig. 2   Side view of arc inside chamber.

the cathode tip is blue-white. Correlation with spectroscopic work[4] indicates that molecular carbon is present in these bright green areas, suggesting ablation of the Plexiglas insulator near the cathode base, while an increase in bremsstrahlung and line intensity is found within a few millimeters of the lateral surface of the cathode and downstream of the cathode tip. Under both photographic and spectroscopic examination, the cathode surface, with the possible exception of a small area at the tip, appears dark. This indicates that most of the cathode surface does not achieve incandescent temperatures, during the time of our experiments, even though the surface current densities exceed 10^7 amp/m². That incandescence should be observable was verified by successfully photographing the filament of a 35 w spot lamp, using the same 5 μsec shutter Kerr-cell system.

Examination of the cathode surface after several hundred firings indicates that melting occurs only at the cathode tip and at scattered small spots, 0.003 in. diam, slightly further back. We find that the surface extends with increasing slope from the initially rounded cathode tip to form a peak 0.1-in. high, surmounted by a globule 0.04 in. in diameter. The surface appears to have been molten along the sides of the peak where slight folds are observed. These indicate flow of material away from the end of the cathode, and thus opposite to the freestream plasma flow. Occasionally, a red spark will be ejected from the arc chamber during or perhaps slightly after the discharge. We may surmise that this results when the cathode tip deforms to the extent that the globule is freed from the peak. Processes then return to normal until the mechanical stability of the peak formation is again lost. Although the current density at the base of the cathode is comparable to that at the cathode tip, no melting is apparent there.

Magnetic Field Distribution

By measurement of the magnetic field distribution within the arc chamber, we obtain both the current flow pattern and the distribution and direction of the $j \times B$ body force. In a quasi-steady discharge, this is accomplished quite simply by use of a small coil of wire placed at the point of interest.[1] As the discharge pattern forms and stabilizes, a current is generated in the coil proportional to the local rate of change of magnetic field. Electronic integration of this signal then allows us to monitor the local magnetic field strength. Cali-
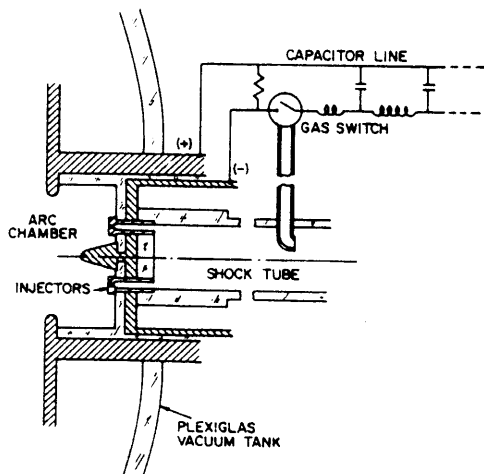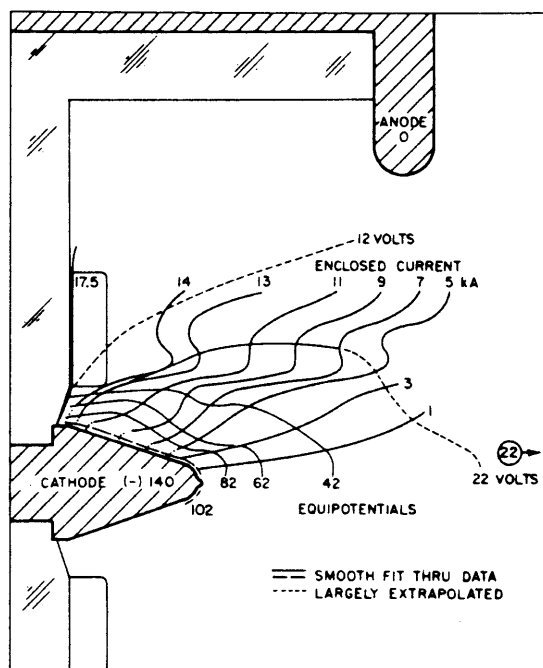

Fig. 1   Accelerator schematic.

Fig. 3 Current streamlines and equipotentials.

bration is accomplished in a situation nearly identical to that in which the probe is used by placing the coil at a position in the chamber where the magnetic field is known, i.e., at a position enclosing the total discharge current.

The result of a survey of the magnetic field in the cathode region is displayed as a plot of enclosed current contours in Fig. 3. Constant fractions of the total arc current flow between these streamlines and the arcjet centerline. The same level and distribution of magnetic field is obtained when the plane of measurement is rotated 90°, in which case the azimuthal position of the magnetic probe relative to the hexagonally arranged gas injectors is different.

We note that 25% of the total current travels in a layer adjacent to the insulator wall, with the remainder of the current distributed in a diffuse manner throughout the cathode region. At the cathode surface, the current density is highest at the tip (5×10^7 amp/m²), somewhat lower at the base of the cathode (4×10^7 amp/m²), and lower still along the intervening slope (1.5×10^7 amp/m²). A rather interesting aspect of the pattern is the double inflection of the current streamlines at the radius of gas injection.

Voltage Distribution

The voltage distribution within the discharge is determined by use of floating electrostatic probes. These measurements

Fig. 4 Twin probe circuit.

accurately reflect the plasma potential distribution, if the electron temperature and plasma flow properties do not vary greatly over the distance of interest. From the potential distribution, we may obtain local components of the electric field in the discharge and, with reference to the current distribution, we may also delineate regions of significant electrical energy deposition.

To minimize the effects of total arc voltage fluctuation from shot-to-shot, we employ two floating probes at nearby positions, separated in either the radial or axial direction. The probe system consists of two No. 18 copper wires, insulated with Mylar and epoxy, and coaxially shielded in the same support tube. The wire ends are exposed to the plasma as nearly spherical tips. Voltages are monitored by three Tektronix P6006 voltage probes, using a Tektronix Type G differential pre-amp to obtain the voltage difference between tips. By simultaneously recording the voltage of one probe and the voltage difference between probes, we obtain the floating potential at two points in the plasma and the average electric field between them.

The equipotential contours resulting from a survey of the cathode region are shown in Fig. 3. The voltage levels of points within the plasma have been corrected from floating potential by subtraction of $\Delta v = (kT_e/2e) \ln(m_{argon}/m_e)$, with kT_e obtained by measurements described in a later section. Note that all voltages are negative, e.g., the cathode voltage is actually minus 140 V.

Power Distribution

From the combined plot of enclosed current contours and equipotentials in Fig. 3, we see the distribution of electrical power within the arc (Table 1). At each area, this is just the product of the current enclosed between adjacent contours and the voltage difference between equipotentials. The total electrical power input to the arc (2.45 Mw) may be apportioned to various regions of the discharge as shown in Table 1. (Note that at the junction of the cathode base and the insulator backwall, the enclosed current is 14 ka; thus 3.5 ka travel very close to the insulator there. Since this insulator is noticeably eroded, we label this area the ablation jet without implying that any set portion of this power is actually delivered to the insulator.)

The main result is that 85% of the total arc power is deposited in the cathode region. We also see that more than a quarter of the total power is involved in the cathode fall. The over-all picture obtained from the field patterns confirms the impression provided by the luminosity distribution: processes in the cathode region are of primary importance to MPD arcjet performance. A detailed analysis of the electromagnetic structure of the discharge in the cathode region is presented in a later section. We must first determine some of the electrical and mechanical properties of our plasma.

Langmuir Probing

Time-resolved local measurements of electron temperature and estimates of electron density are obtained using a twin Langmuir probe technique. Previously,[3] a single Langmuir probe consisting of a 0.003-in.-diam, 0.12-in.-long tungsten
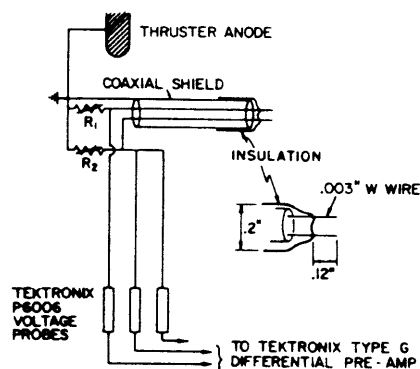
Table 1 Power distribution in arc

	ΔV	J_{en}	% Total power	Cathode region power
Cathode fall	38	17.5 ka	27.0%	
Ablation jet	90	3.5 ka	13.0%	85.7%
Cathode plasma	80	14.0 ka	45.7%	
Elsewhere in arc chamber			14.3%	

wire, aligned parallel to the plasma flow, was used to measure electron temperature and density in the downstream exhaust jet. The procedure employed was to monitor the voltage across a resistor connecting the probe tip to ground, and thereby to obtain both the current drawn by the probe and the probe voltage during quasisteady operation with a single measurement. Repetition of this procedure with a succession of resistor values on a shot-by-shot basis, provided the probe characteristic. Application of this technique within the arc chamber, however, was not successful because the variations in local plasma potential from shot-to-shot exceeded the range of the transition portion of the probe characteristic.

To overcome this difficulty and also to obtain results more readily, we utilize two identical single Langmuir probes, of dimensions similar to those used previously, mounted in the same support tube and sampling essentially the same plasma (see Fig. 4). Resistors of different values connect the probe tips to ground, so that different currents are drawn and the probe tips are established at different voltages. We thus simultaneously obtain two points on the same probe characteristic. If we operate on the transition portion of the characteristic, at a level where the ion current to the probe tips may be neglected ($I \approx I_e$), then the ratio of currents drawn by the tips is related to the voltage difference between tips by a Boltzmann factor based on the electron temperature

$$I_2/I_1 = e^{-(V_2 - V_1)/kT_e}. \qquad (1)$$

Measurement of this voltage difference, and the voltage of either tip provides the ratio of probe currents. The local electron temperature is then

$$kT_e = \Delta V/\ln(I_2/I_1) \qquad (2)$$

This is essentially the inverse of the slope of a line between two points on the transition branch of a plot of $\ln I$ vs V. If, however, one or both of the probe tips is on the electron saturation branch, the computed value of kT_e will be much larger than the true value. Thus, we may ascertain the position of our probe tips with respect to the probe characteristic by noting the variation of the computed value of kT_e with the highest current drawn by our system as we change resistor pairs. Values of kT_e should be the same if both tips are on the transition portion of the characteristic, while a sharp increase occurs when the highest current drawn exceeds the saturation electron current to a probe tip. In Fig. 5 this behavior is shown at a representative position within the arc chamber. Figure 6 displays the variation of kT_e with time during quasi-steady operation.

The upswing or "elbow" in Fig. 5 signals that one probe tip is drawing saturation electron current. From the measured current to that tip, and the electron temperature determined from the level portion of the curve, we may estimate the local electron density. The strong magnetic field in the cathode region will cause the probe characteristic (current-voltage diagram) to plateau before reaching the true saturation electron current, so electrostatic probe data provide only minimum values of the electron density near the cathode. Indeed, later analysis based on the electromagnetic structure of the discharge indicates electron densities almost an order of
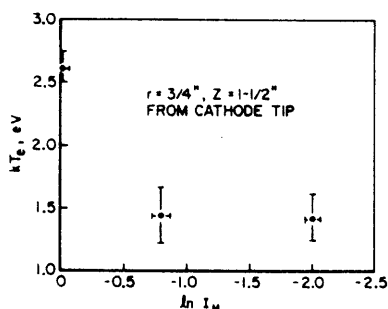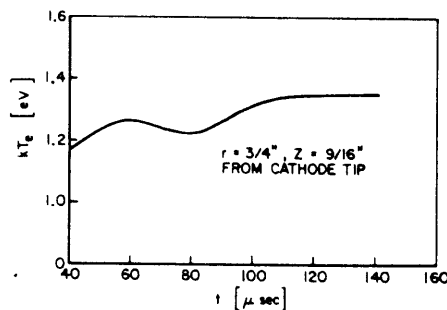

Fig. 6 kT_e during quasi-steady operation.

magnitude higher than values obtained by these probes. The electron temperature measurement should not be affected by the presence of the magnetic field since it is based on the transition portion of the characteristic. Collisional effects near the probe surface also tend to distort the results obtained from probe data. Computations based on the higher densities obtained from analysis of the discharge structure indicate that $\lambda_{ei}/r_p \approx 1$, $\lambda_D/r_p \approx 10^{-3}$; where λ_{ei} is the electron-ion MFP, λ_D is the Debye length, and r_p is the probe radius. The work of Kirchhoff et al.[5] suggests that transition flow effects are, therefore, unimportant in our probe situation.

In Fig. 7 we display values of electron temperature and estimates of electron density obtained using the twin probe technique at various points within the arc chamber. We note that the electron temperature is nearly constant throughout the arc chamber and downstream exhaust, whereas the electron density varies by three orders of magnitude from the gas injectors to the cathode tip. Values of kT_e and n_e provided by the twin probe method in the downstream exhaust are nearly identical to those previously obtained by the more tedious single Langmuir probe technique, indicating the utility of this new approach as an electron temperature probe. Measurements of kT_e and n_e just downstream of the cathode tip were obtained from data accumulated by sacrificing the probe tips there after a series of experiments was completed elsewhere in the chamber. The 0.003-in.-diam tungsten probe tips would survive 20–40 firings within the arc, except near the cathode tip, where they are lost during the sub-

Fig. 5 Computed kT_e vs highest current to probe tip.
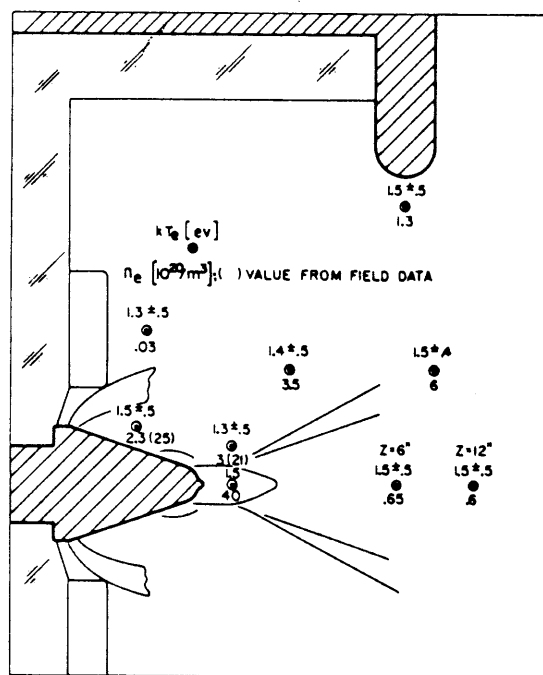

Fig. 7   Electron temperatures and densities from twin probe data.

sequent discharges associated with ringdown of the capacitor bank power supply. As we mentioned above, the estimates of electron density shown in Fig. 7 provide minimum values which other data indicate should be corrected upwards by about a factor of 10 in the cathode region.

III. Analysis of the Experimental Results

Nature of the Cathode Plasma

The minimum levels of electron density provided by the twin probe data will now be used to establish the quasi-neutral, continuum nature of our plasma and thereby to justify a priori the MGD formulation from which the higher density values are obtained. An important parameter characterizing a plasma is its ionization level, α. For an input argon mass flow of 5.9 g/sec, we estimate that the total heavy-particle density in the back portion of the arc chamber is about $10^{22}/m^3$, where we assume that the flow expands from the injector orifices over the entire backwall to a speed of about 10^3 m/sec. This density decreases by about a factor of 10 downstream of the cathode tip, where we expect plasma speeds on the order of 10^4 m/sec, based on a downstream exhaust speed of about 2×10^4 m/sec. Comparing these densities with our estimates of electron density from the twin probe data, we find that the minimum ionization level progresses from a few percent near the backwall of the chamber to some tens of percent near the cathode surface and downstream of the cathode tip. The electrical conductivity of the plasma in the cathode region is then found[6] to be $\sigma_0 = 8(\pm 5) \times 10^3$ mho/m, for $kT_e = 1.5 (\pm 0.5)$ ev and $0.03 \leq \alpha \leq 1$.

Using our estimates of electron density, we may compute various distances that characterize the plasma flow. In particular, we find[7] that the Debye length is much smaller than any distance of interest, so we are always dealing with a quasi-neutral plasma (except in electrode and probe sheaths). Also, we find that the mean free paths for electron-ion, ion-ion, and ion-atom momentum and energy transfer collisions are all small compared to the dimensions of the cathode region. Both the electron Hall parameter and the magnetic Reynolds number exceed unity in the cathode region indicating significant interaction of the plasma flow and the discharge current pattern. A factor of 10 increase in electron density will decrease the various MFP's computed by a similar factor so that the continuum aspects of the plasma flow are enhanced. Thus, we see from our computations that a magnetogasdynamic formulation is appropriate in the cathode region.

Generalized Ohm's Law Basis for the Electric Field

The electric and magnetic fields in a discharge may be related to the current and plasma flows through a generalized Ohm's law

$$\mathbf{j} = \sigma_0[\mathbf{E} + \mathbf{u}_e \times \mathbf{B} + \nabla p_e/n_e e] \tag{3}$$

It is common to express the current density as a function of electric field as we have done. The independent variable in our operation, however, is the current level. The voltage distribution is determined by the conductivity, magnetic field and plasma flow that result at this current level, for a given particle (and mass) density. That is, the electric field in the plasma arises from a need to conduct current in the presence of collisions, magnetic fields, and pressure gradients. Since we measure $\mathbf{E}$ experimentally, however, we shall use it as an independent variable along with $\mathbf{B}$ and $\mathbf{j}$ to obtain the plasma flow from the electromagnetic structure of the discharge.

Electron Motion

Components of the electron velocity parallel and perpendicular to the current flow may be obtained from the vector and

scalar products respectively of $\mathbf{j}$ with the above Ohm's law. We have[7]

$$u_{e\parallel} = -E_\perp'/B$$

and

$$u_{e\perp} = \frac{E_\parallel' - j/\sigma_0}{B} \tag{4}$$

where

$$\mathbf{E}' = \mathbf{E} + \nabla p_e/n_e e \tag{5}$$

Note that "$\parallel$" and "$\perp$" refer to the current density direction not the magnetic field vector. Thus, $u_{e\perp} = u_{i\perp}$ since $j_\perp \equiv 0$. The other component of ion velocity is related to $\mathbf{u}_e$ through the current density:

$$u_{i\parallel} = j/n_e e + u_{e\parallel} = j/n_e e - E_\perp'/B \tag{6}$$

Relations between electron motion and field structure of such simple form are normally found only in certain special situations. For example, $u_e = E/B$ is obtained for collisionless, cross-field drift. Our results obtain because of the special way we have chosen components. The current density, magnetic field, and $\mathbf{j} \times \mathbf{B}$ force vectors in this sense provide a natural coordinate system for an MPD discharge. The usefulness of these formulas derives from our experimental knowledge of the electromagnetic structure of the discharge. We are in reality solving the problem in reverse. The current density, ion velocity and particle density define the electron motion. The magnetic field and pressure distributions are also coupled to the geometry of current conduction and the mechanics of ion flow. The electric field distribution is a result of this dynamical system.

Ion Motion

This viewpoint is particularly important in understanding ion acceleration and current conduction. We may write the ion momentum equation as

$$n_i m_i(\mathbf{u}_i \cdot \nabla)\mathbf{u}_i = n_i e[\mathbf{E} + \mathbf{u}_i \times \mathbf{B}] - \nabla p_i + n_e m_e(\mathbf{u}_e - \mathbf{u}_i)\nu_c{}^p + \mathbf{P}_{iA} \tag{7}$$

where $V_c{}^p$ is the frequency of momentum transfer collisions between electrons and ions, and $\mathbf{P}_{iA}$ is the collisional force between ions and atoms. Substituting for the electric field, we have

$$n_i m_i(\mathbf{u}_i \cdot \nabla)\mathbf{u}_i = \mathbf{j} \times \mathbf{B} - \nabla(p_i + p_e) + \mathbf{P}_{iA} \tag{8}$$

It is important to note that in this equation the net electrical force acting on the ion fluid is the $\mathbf{j} \times \mathbf{B}$ force. Neglecting pressure gradients, ions will participate in current conduction only insofar as the $\mathbf{j} \times \mathbf{B}$ force in one part of the discharge accelerates them parallel to the current density vector further downstream. Examining our current pattern, we see that, on the whole, the $\mathbf{j} \times \mathbf{B}$ vector does not change direction much in the cathode region, except in the immediate vicinity of the cathode surface. This indicates that ion motion will always tend to be normal to the current flow and therefore electron current will predominate. We investigate this further by considering the ion kinetic energy.

Returning to the ion momentum equation, we include the effects of ion-atom collisions by addition of the atom momentum equation

$$n_A m_A(\mathbf{u}_A \cdot \nabla)\mathbf{u}_A = -\mathbf{P}_{iA} - \nabla p_A \tag{9}$$

Assuming good coupling between ions and atoms, based on our previous computations, so that $\mathbf{u}_A \cong \mathbf{u}_i$, we have

$$nm_i(\mathbf{u} \cdot \nabla)\mathbf{u} = (n_e/\alpha)m_i(\mathbf{u} \cdot \nabla)\mathbf{u} = \mathbf{j} \times \mathbf{B} - \nabla(p_i + p_e + p_A) \tag{10}$$

where α again denotes the ionization level.

The kinetic energy of a heavy particle due to acceleration by the $\mathbf{j} \times \mathbf{B}$ force is then (in volts)

$$\mathcal{E} = \int (jB/ne)dx_\perp = \int \alpha(jB/n_e e)dx_\perp \qquad (11)$$

The maximum energy acquired by an ion occurs when $\alpha = 1$.

If the electrons carry all the current, we have $u_{e\parallel} = j/n_e e$, so $jB = n_e e E_\perp$. The maximum kinetic energy of an ion is then

$$\mathcal{E}_{max} = \int E_\perp \, dx_\perp = \int_{\text{along } x_\perp} \mathbf{E} \cdot \mathbf{dl} = (V - V_0)_{\text{along } x_\perp} \qquad (12)$$

Thus, if $j = j_e$, the maximum ion kinetic energy is just the voltage difference along its path, i.e., along a path normal to the current flow. On the other hand, in the case of strictly ion current, the maximum kinetic energy is obtained when the ion motion is collisionless, since energy is otherwise lost to electrons and atoms. This maximum kinetic energy is also given by the voltage difference along the ion's path from its point of origin. If we assume that ions are all created at the same potential V_0 in the low field region near the injectors (since this provides the maximum voltage difference), then the maximum ion kinetic energy at any point is determined by the local voltage. (This applies only in our high electric field region near the cathode where we may neglect electron pressure gradients compared to $E_\perp$.)

From the measured distributions of electric and magnetic field and current density, we compute the electron speed normal to the current flow. Since this is also the ion speed in that direction, we may therefore calculate the kinetic energy associated with ion motion normal to the current flow. We also know the voltage at the same location, so we can compare this kinetic energy with the maximum possible ion kinetic energy. In this way, we may assess the division of ion energy into motion parallel and perpendicular to the current flow. We find that ion motion normal to the current flow accounts for essentially all the ion kinetic energy, and conclude that little energy is associated with ion motion parallel to the current flow. This confirms our previous impression based on the geometry of the current pattern. Thus, the region between the gas injectors and the immediate vicinity of the cathode surface and jet is characterized by electron current conduction in a tensor manner. Ion flow paths are shown in Fig. 8, along with the ion speed at various stations. It is assumed here that $\alpha = 1$, so that with $j = j_e$, the ion energy is just

$$\mathcal{E}_i = \int (jB/n_e e)dx_\perp = (V - V_0)_{\text{along } x_\perp} \qquad (13)$$

It is important to note that our integration terminates near the centerline or cathode surface, since pressure gradients must be included there. Above all, observe that the relation between ion kinetic energy and voltage obtains only along a trajectory parallel to the $\mathbf{j} \times \mathbf{B}$ force. Again: the net electrical force on the ion fluid is the $\mathbf{j} \times \mathbf{B}$ force, not the gradient in electric potential. The ion does not lose its kinetic energy in leaving the vicinity of the cathode as would be implied by a
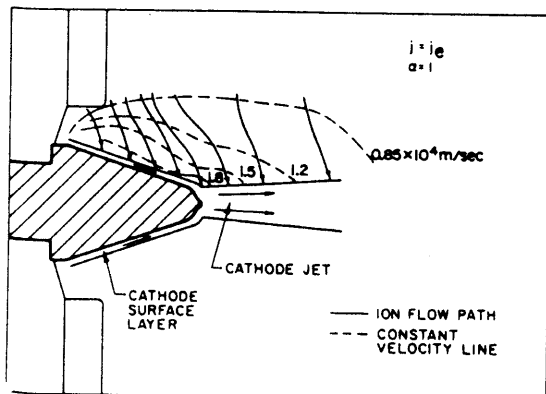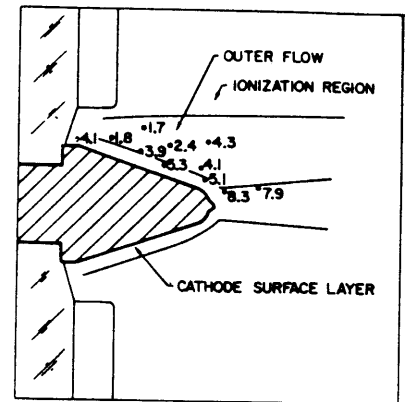
Fig. 9 Electron densities from field data, $10^{21}/\text{m}^3$.

collisionless, electrostatic acceleration model. In particular, the force exerted on the ion by the electric field in the cathode jet is exactly balanced by the collisional force of electrons.

Cathode Plasma Revisited

Given that all the current in the cathode region is carried by electrons, we may calculate the electron density from the field data. We have

$$j = j_e = n_e e E_\perp/B, \quad \text{so} \quad n_e = jB/eE_\perp \qquad (14)$$

Using this formula, we compute electron densities that are about an order of magnitude higher than our estimates based on the electrostatic probe data. Note that the electron velocities parallel to the current, $E_\perp/B$, are everywhere greater, by a factor of at least three, than the maximum ion velocities so that any ion contribution to current conduction will not greatly affect the plasma densities obtained from the preceding formula. Such densities are displayed in Fig. 9 at various positions within the cathode region. Our results are in good agreement with spectroscopic evidence recently obtained with a longer duration current pulse.[2] These values from the field data suggest that about half the input mass is involved in the flow to the cathode surface. The remaining mass is accelerated to the cathode jet or directly downstream (pumping and blowing modes).[3]

Our computations indicate that the charged-particle density does not vary greatly through the cathode region except near the gas injector flow and near the cathode surface and jet. Since the electron temperature is also rather uniform, electron pressure gradient effects may be neglected in most of the cathode region. Where such effects are important, our calculations, based only on the field data, exhibit difficulties. For example, the electrical conductivity computed from the electromagnetic structure is somewhat less than that calculated previously from the electron temperature everywhere in the cathode region except near the radius of gas injection ($r \approx 2$ cm) and near the cathode surface, where very high to infinite values are obtained. Thus, within a few millimeters of the cathode surface, we must re-examine the plasma flow and discharge structure.

Cathode Surface Layer

From the previous analysis, we find that a high-speed plasma flow is delivered to the immediate vicinity of the cathode surface. This flow has a velocity comparable to that measured in the downstream exhaust jet ($\sim 2 \times 10^4$ m/sec) and is directed, for the most part, radially inward. Pressure gradients near the cathode surface and in the cathode jet are required to deflect this flow into an axial, thrust producing, direction. This situation recalls the "pumping mode" of MPD arcjet operation.[3] In our case, this process is not confined to the cathode jet but extends upstream over the lateral surface of the cathode, where the "pumped" plasma is also accelerated by a $\mathbf{j} \times \mathbf{B}$ force along the cathode surface. We

Fig. 8   Plasma flow in cathode region.

now continue the analysis of the discharge and plasma flow in a layer, a few millimeters thick, adjacent to the cathode surface. We utilize a different approach to the experimental data within a distance $h \cong 2.5$ mm of the cathode because our previous analysis leads to some difficulties there and because the resolution of our experiment does not permit the same detailed consideration as before.

MGD Analysis Including Pressure Gradients

It may be shown[7] that the current flow pattern is scalar if the magnetic Reynolds number based on the electron flow speed is small compared to unity. At the edge of the surface layer, we have $R_{me} = \mu_0 \sigma_0 u_e L \approx 0.28$ (with $\sigma_0 \approx 5$ kmho/m, for $kT_e = 1.5$ ev; $u_e \approx 1.8 \times 10^4$ m/sec and $L = h \cong 2.5$ mm). Thus, the current flow lines should enter the cathode normal to the surface. Within the cathode surface layer, we shall therefore simplify our problem by assuming j and E are both perpendicular to the surface (and are thereby parallel). We have then

$$uB = E - j/\sigma_0 + (1/n_e e)(\partial p_e/\partial x_\parallel) \quad (15)$$

where u is the plasma flow speed along the cathode surface. With $E = \partial V/\partial x_\parallel$, since all voltages are negative in our experiment, and $(1/n_e e)(\partial/\partial x_\parallel)p_e \cong (\partial/\partial x)(kT_e \ln n_e)/e$, assuming, kT_e is about constant, we obtain

$$\int uB dx_\parallel = \Delta V + (kT_e/e) \ln(n_e/n_c) - \int j dx_\parallel/\sigma_0 \quad (16)$$

Now, with B, j and $\sigma_0 = \sigma_0(T_e)$ all about constant in the surface layer, the average velocity of the flow along the surface is approximately

$$\mathbf{u} = \frac{1}{h} \int u dx_\parallel \cong [\Delta V + (kT_e/e) \ln n_e/n_c - jh/\sigma_0]/Bh \quad (17)$$

In this way, we are using our measurements of electric and magnetic fields and current density near the cathode surface as a type of MHD channel flow meter. We measure the voltage across the flow, correct for the resistive voltage drop and pressure gradients to obtain the back EMF, and then compute u from the known (measured) magnetic field strength.

The density within the surface layer reflects the influx of plasma from the outer flow. Neglecting mass addition at the cathode shoulder, we have

$$\int \rho u (2\pi R) dx_\parallel = \int \rho_c u_c (2\pi R) dx \quad (18)$$

where x is measured along the cathode slope and $\rho_c u_c$ is the mass influx from the outer flow. Since we are interested merely in the characteristic densities in the surface layer, we shall neglect the variation of $\rho_c u_c$ and R with x. We then have

$$\bar{\rho} \cong \rho_c u_c x/\mathbf{u}h$$

so $\quad (19)$

$$n_e = \frac{(\rho_c/m_i)u_c Bx}{\Delta V + kT_e/e \ln(n_e/n_c) - (jh/\sigma_0)}$$

which may be solved by iteration for n_e. In a similar spirit, the over-all energy equation of the surface layer flow is

$$\rho u h [\theta(T) + \tfrac{1}{2}\mathbf{u}^2] = [j\Delta V + q_p + \rho_c u_c u_0^2/2]x \quad (20)$$

where $\theta(T)$ is the enthalpy of the flow; $j\Delta V$ is the electrical power deposited; q_p is the energy transfer from the cathode fall zone; and $\rho_c u_c u_0^2/2$ is the energy flux from the outer flow. With $\rho u h \approx \rho_c u_c x$, we have

$$\theta(T) = j\Delta V + q_p/\rho_c u_c - (\mathbf{u}^2 - u_0^2)/2 \quad (21)$$

Solving these equations,[7] we find that the average flow speed ($\mathbf{u} \approx 1.5 \times 10^4$ m/sec) is comparable to that of the flow prior to deflection. Both the density ($n \approx 3 \times 10^{22}$ m^{-3})

and heavy-particle temperature ($T_H \approx 4$ ev) increase above their values in the outer flow (where $T_H \leq T_e \cong 1.5$ ev), confirming the existence of a pressure gradient at the cathode surface. The heavy-particle temperature was estimated from the enthalpy by assuming equilibrium conditions in the surface layer. Computations of the time for equipartition t_{eq} (Ref. 9) between ions and electrons at these densities, for $kT_e = 1.5$ ev, indicate that energy transfer from ions to electrons is quite efficient ($\mathbf{u}t_{eq} \approx 1$ mm), so that the electron fluid acts as a heat conductor between the high (kinetic) temperature ions and their excited states. The high effective specific heat of this system serves to keep heavy-particle temperatures near the cathode surface at the moderate levels indicated by the equilibrium calculations. Recent spectroscopic evidence,[2] with a longer pulse of comparable total current level, indicates that the plasma density indeed increases from about 3×10^{21}/m^3 in the outer flow to about 2×10^{22}/m^3 in a few millimeter thick layer adjacent to the cathode surface. At higher mass flows (36 g/sec), preliminary spectroscopic data has been obtained, yielding estimates of heavy-particle temperature from 2 to 4 ev just downstream of the cathode tip. These data thus tend to confirm the results of our approximate analysis.

Extrapolating our calculations to the vicinity of the cathode tip, we find[7] that a hypersonic ($M \approx 5$) flow is obtained, suggesting that in the same manner as flow behind a hypersonic blunt body, the abrupt convex termination of the cathode may cause boundary-layer separation. The annular surface layer flow will thus overshoot the end of the cathode and collapse on the arcjet centerline a few tip diameters downstream. A portion of this flow stagnates there and the resulting high-pressure region induces a reverse flow toward the cathode. Such a situation was previously indicated by the molten surface flow at the cathode tip. The rest of the plasma flow from the surface layer is turned parallel to the arcjet centerline. The compression waves involved coalesce to form a trailing shock as suggested by the sharply defined luminous cone in Fig. 2.

Cathode Fall Zone

The energy transfer to the surface layer flow from the cathode fall zone q_p is computed[7] from a model for the cathode fall based on energy balances at the cathode surface and in the local plasma. Briefly, with a no-slip assumption appropriate to the continuum flow in the surface layer, the energy transfer to the cathode surface by ion bombardment is essentially $j_i(V_f + \epsilon_i - \phi_w)$, where $(\epsilon_i - \phi_w)$ is the energy deposited by an ion at the surface upon recombination. This energy flux must be balanced by heat conduction to the cathode interior, an unsteady process in our experiment, and by emission of electrons. That is

$$j_i(V_f + \epsilon_i - \phi_w) = q_c + j_e\phi_w \quad (22)$$

The emitted electrons accelerate through the cathode fall and deposit an energy $j_e V_f$ in the local plasma. Part of this energy is needed to re-ionize the heavy particles returning to the local plasma from the cathode surface. The remainder q_p is available for excitation, ionization, and heating of the flow in the surface layer. That is

$$j_e V_f = j_i\epsilon_i + q_p \quad (23)$$

Other features of this model are the following: the heavy-particle temperature in the local plasma is equal to the surface temperature (no-slip condition) because of collisional equilibration with the neutral atom flow returning from the surface. The plasma pressure immediately adjacent to the cathode surface is therefore just the electron pressure. The charged-particle density must be such that the electron pressure balances the normal momentum flux to the cathode surface layer from the outer flow. With kT_e again about 1.5 ev, limited by inelastic cooling processes, densities on the order

$10^{23}/m^3$ are computed. The random ion flux $n_i c_i/4$, and therefore the ion current in the cathode fall, is determined by the surface temperature ($T_i \approx T_w$, $n_i = n_e$) and the magnitude and direction of the momentum flux to the cathode surface layer. Suffice to say here, that 1) approximately half of the electrical power involved in the cathode fall is delivered to the surface flow (q_p), the remainder is lost to heating the cathode (q_c) and removing electrons which later heat the anode ($j_e \phi_w$); 2) the cathode surface temperature is quite low, on the order of 400–500°K, a result consistent with the photographic evidence and clearly precluding thermionic emission. Even at temperatures above the melting point of tungsten, thermionic or field enhanced thermionic (T/F) emission mechanisms[10] cannot account for the observed current densities along the cathode slope. Some form of individual field (I/F) emission mechanism[11,12] is suggested.

IV. Review and Summary

The physical picture obtained from the experiments and analysis is that a highly ionized plasma is created within one base diameter of the cathode surface and accelerated to the immediate vicinity of the cathode by the $\mathbf{j} \times \mathbf{B}$ force. This force is transmitted from the current-carrying electrons to the ions by an electric field normal to the current flow. The kinetic energy obtained by a heavy particle in this way is given by the voltage difference along its path normal to the current. Since this voltage is comparable to that along the current flow in a tensor conduction situation, ion kinetic energies proportional to the arc voltage drop should be observed even in the absence of ion current.

Near the cathode surface, a high-density layer exists in which pressure gradients balance the normal momentum flux to the cathode, while a $\mathbf{j} \times \mathbf{B}$ force accelerates the plasma along the surface. In this way, the flow to the cathode is deflected axially downstream. The heat generated by this deflection process and the energy delivered to the plasma from the cathode fall increases the enthalpy of the plasma, but the heavy-particle temperature remains moderate because of the high effective specific heat associated with inelastic processes such as excitation and ionization. Recovery of this energy, and indeed of any electrothermal input to the plasma, to increase the arcjet exhaust velocity appears doubtful since the uniformity of the electron temperature in the presence of high fields and/or higher ion temperatures suggests that cooling of the flow by inelastic events continues well downstream of the arc chamber.

Rather than the high pressure "pumped" plasma core previously thought to exist at the cathode tip, a high pressure, high velocity layer is found along the lateral surface of the cathode. Boundary-layer separation and flow recirculation may occur near the cathode tip allowing most of the flow from the surface to exit the cathode region as a thin annulus, escaping both stagnation point and shock wave interactions.

In terms of the electric field within the plasma, we may consider that the outer flow region within a diam of the cathode behaves like a Hall field accelerator, while in the cathode surface layer, the tensor character of current conduction is diminished so the electric field there resembles that in an MGD channel accelerator. In the cathode jet and plume, we merely have the resistive field as in an electrothermal device, coupled with an electromagnetic nozzle. Thus, our MPD arcjet incorporates three basic types of electric thruster in different portions of the discharge.

References

[1] Clark, K. E., "Quasi-Steady Plasma Acceleration," Report No. 859, Dept. of Aerospace and Mechanical Sciences, May 1969, Princeton Univ., Princeton, N.J.

[2] Clark, K. E., Di Capua, M. S., Jahn, R. G., and Von Jaskowsky, W. F., "Quasi-Steady Magnetoplasmadynamic Arc Characteristics," AIAA Paper 70-1095, Aug. 31–Sept. 2, 1970, Stanford, Calif.

[3] Jahn, R. G. et al., "Acceleration Patterns in Quasi-Steady MPD Arcs," AIAA Paper 70-165, Jan. 19–21, 1971, New York.

[4] Von Jaskowsky, W. F., private communication, 1970, Princeton Univ., Princeton, N.J.

[5] Kirchhoff, R. H., Peterson, E. W., and Talbot, L., "An Experimental Study of the Cylindrical Langmuir Probe Response in the Transition Regime," AIAA Paper 70-85, 1970, New York.

[6] Nighan, W. L., "Electrical Conductivity of Partially Ionized Noble Gases," *The Physics of Fluids*, Vol. 12, No. 1, Jan. 1969, pp. 162–171.

[7] Turchi, P. J., "The Cathode Region of a Quasi-Steady MPD Arcjet," Ph.D. dissertation, Rept. 940, Oct. 1970, Dept. of Aerospace and Mechanical Sciences, Princeton Univ., Princeton, N.J.

[8] Jahn, R. G., *Physics of Electric Propulsion*, McGraw-Hill, New York, 1968, Chap. 8.

[9] Spitzer, L., Jr., *Physics of Fully Ionized Gases*, Interscience, New York, 1962, Chap. 5.

[10] Lee, T. H., Greenwood, A., Breingan, W. D., and Fullerton, H. P., "An Analytical Study of the Physical Processes in the Cathode Region of an Arc," OAR Rept. ARL 66-0065, April 1966, General Electric Co., Philadelphia, Pa.

[11] Ecker, G., "Electrode Components of the Arc Discharge," *Ergebnisse der exakten Naturwissenschaften*, Vol. 33, Springer-Verlag, Berlin, 1961.

[12] Aisenberg, S., Hu, P., Rohatgi, V., and Ziering, S., "Plasma Boundary Interactions," NASA CR-868, Aug. 1967, Space Sciences, Inc., Waltham, Mass.